World Electric Vehicle Journal

MDPI

Article

Analysis of Coil Parameters and Comparison of Circular, Rectangular, and Hexagonal Coils Used in WPT System for Electric Vehicle Charging

Tasnime Bouanou *, Hassan El Fadil, Abdellah Lassioui, Ouidad Assaddiki and Sara Njili

Ingénierie des Systèmes Avancés (ISA) Laboratory, ENSA, Ibn Tofail University, Kenitra BP 242, Morocco; elfadilhassan@yahoo.fr (H.E.F.); abdellah.lassioui@uit.ac.ma (A.L.); assaddiki.ouidad4@gmail.com (O.A.); njilisara@gmail.com (S.N.)

* Correspondence: Bouanou.t@gmail.com

Abstract: In this paper, the major factors that affect the performance of wireless power transfer systems, such as coil inner radius and coil number of turns, are discussed. A comparison of three coil shapes covering the coreless case, the case with ferrite, and the case with ferrite and aluminum is also carried out. Another comparison is proposed by addressing the combination of different coil shapes in the wireless power transfer (WPT)system. The analysis covers the coupling coefficient, the mutual inductance, and the self-inductance. Due to the complexity of calculating these parameters, the finite element analysis (FEA) method is adopted by using the Ansys Maxwell software. An introduction to the typical WPT system for electric vehicle charging is also presented.

Keywords: electric vehicle (EV); wireless power transfer (WPT); magnetic resonant WPT; finite element analysis (FEA); coupling coefficient; shielding; mutual inductance; self-inductance; Ansys Maxwell

Citation: Bouanou, T.; El Fadil, H.; Lassioui, A.; Assaddiki, O.; Njili, S. Analysis of Coil Parameters and Comparison of Circular, Rectangular, and Hexagonal Coils Used in WPT System for Electric Vehicle Charging. *World Electr. Veh. J.* **2021**, *12*, 45. https://doi.org/10.3390/wevj12010045

Received: 7 January 2021
Accepted: 13 March 2021
Published: 17 March 2021

1. Introduction

As the large demand for fossil fuels for road transportation continues to grow and the percentage of pollution coming from conventional vehicles increases, the need for an alternative solution has become a major necessity. The electric vehicle presents a suitable solution for road transportation by offering multiple advantages: zero gas emissions, reduced noise pollution, low maintenance, and lower running costs [1].

The biggest challenge that electric vehicles face is the battery pack capacities, which give a short driving range because of their limited life and high cost [2]; currently, the battery charging operation for the electric vehicle is carried out by the charging cables. On the other hand, the wireless power transfer system charging method is already used in a variety of systems and applications, such as biomedical devices, industrial manufacturing, including robotic platforms, and a few consumer electronics (watches, smartphones, etc.) [3].

The magnetic resonant wireless power transfer (WPT) technology is a method proposed by Kurs [4] where the energy is wirelessly transferred between the transmitting coil and the secondary coil under resonant conditions. It is suitable for electric vehicle applications. The electric vehicle wireless charging operation is carried out in stationary or dynamic mode. In the first mode, the vehicle is parked whereby the transmitting coil is parallel to the receiving coil. Then, the charging operation can be started. In the second mode, the vehicle is charged while moving on the road occupied by transmitting coils. Thereby, the wireless charging method is easier, with no need for human intervention, safer, and needs less maintenance compared to the conductive method. However, the wireless charging method presents some drawbacks—for example, the large distance between the transmitting and receiving coil, resulting in low coupling and human safety due to the exposure to the magnetic field. The coil design is one of the crucial factors in designing

a wireless charging system. The coil system in the stationary charging mode is designed in pad form. Several coil shapes are proposed in the literature. Circular and rectangular shapes are the most common structures used in electric vehicle (EV) chargers due to their simplicity. Furthermore, Auckland University [5] proposed a DD coil structure. In addition, other structures have been proposed, such as flux pipe couplers [6], DD-Q derived from DD, bipolar pads [7], Tripolar pads, and more [8,9]. The design of the pad is a crucial exercise during the charger design process; the system is required to have a large air gap, misalignment tolerance, high coupling and efficiency, and light weight. The objective is to increase the coupling and efficiency and reduce the leakage flux between the transmitting and receiving pads. The coil parameters have a significant effect on the performance of the coil; this effect includes the coupling coefficient, the mutual inductance, and the coil inductance. Moreover, ferrite and aluminum are usually used to guide the flux and reduce the leakage flux, respectively. Although the introduction of these materials enhances the coupling values, the pad weight remains a crucial element during the pad conception.

The influence of the coil's number of turns and the coil's inner radius variation on system coupling is investigated in [10]. The simulation results of the coupling coefficient were collected by varying the number of turns of the transmitting coil. The same results were collected for the coil inner radius. However, the study did not take into account the variation in the receiving coil parameters and the simulation results of the coil inductance and mutual inductance. In [11], a comparison between three coil shapes was carried out, using the same frequency; the simulation results of helix, planar spiral, and square helix coils indicate that the helix coil has the highest efficiency while the planar spiral has the lowest one. However, the flat coil is the most widely adopted for electric vehicle charging applications in order to reduce the pad thickness. In [12], a comparison between the popular coil shapes and the effects of coil parameters such as the number of turns, pitch, and inner and outer diameter on the efficiency of the coil is conducted. However, no simulations have been conducted to analyze these parameters and to perform a comparison between coils. In [13], a simulation study was carried out to explore the variation in the coupling coefficient for different coil shapes under different air gaps and coil misalignments. However, the variation in the coil inductance was not discussed. In the same context, [14] presents a cost-effectiveness comparison of three shapes—rectangular, circular, and hexagonal—based on the efficiency, the horizontal misalignment, the flux density, and the output power. However, the number of turns and the width of the three couplers are different and a comparison according to the coupling coefficient and self-inductance was not conducted. Several studies [15–18] have been carried out to compare various coil topologies. Thus, in these comparisons, the transmitting coil and the receiving coil have the same shape. However, various situations can be encountered in the charging stations because the receiving coil differs from one vehicle to another and the transmitting coil of each charging station can be different.

This paper highlights the principal impacts of a coil's main structural parameters, such as coil inner radius and coil number of turns, on the WPT system's performance, and it also considers the influence of the introduction of ferrite and aluminum into the system. Moreover, a comparison of three coil shapes covering a coreless case, a case with ferrite, and a case with ferrite and aluminum is carried out. Another comparison is proposed covering nine possibilities that can be encountered in wireless charging operations using the same three shapes. The analysis covers the self-inductance, the coupling coefficient, and the mutual inductance between the transmitting and receiving coils.

The flow of this document is organized as follows: Section 2 presents the typical WPT system for electric vehicle charging. Section 3 describes the impacts of coil structure and coil position on the WPT systems performance, including the two-coil vertical position, the influence of ferrite and aluminum, the coil inner radius, and the number of turns. Section 4 is devoted to the comparison of three coil topologies, including the introduction of ferrite and aluminum for the topologies that have similar transmitting and receiving coils. Moreover, nine mixed topologies are also compared and analyzed. The analysis

covers the self-inductance, mutual inductance, and the coupling coefficient. Section 5 provides a conclusion to the present paper.

2. The Typical WPT System for Electric Vehicle Charging

2.1. WPT System Basic Principles

The electric vehicle presents a perfect solution for green transportation. However, the major downside of this type of vehicle is related to the energy storage technology. The wireless charging technology offers multiple advantages towards the battery weight, cost, and size. Figure 1 illustrates the concept of WPT charging for the electric vehicle. The WPT system is enabled when the electric vehicle enters the charging zone. The energy is transferred then wirelessly from the power source to the battery of the vehicle using the magnetic field created between the transmitting coil and receiving coil.

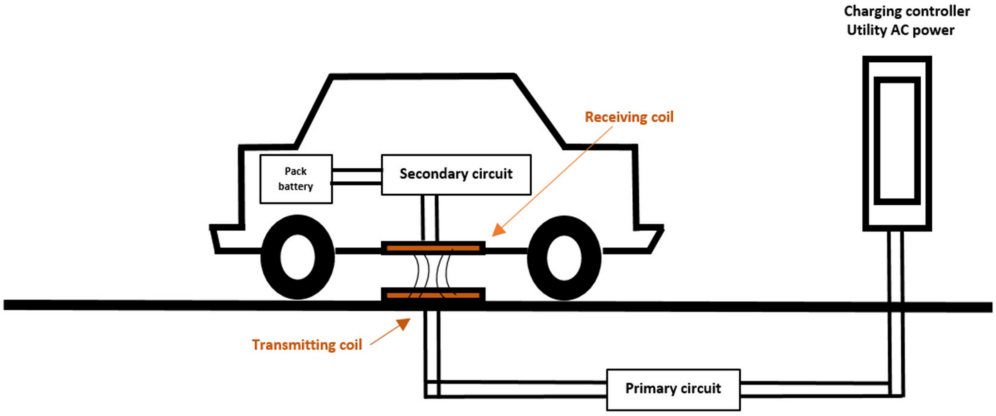

Figure 1. The concept of WPT charging for the electric vehicle.

The charging system is composed of two parts: the on-board and the off-board parts. The first one is located on the vehicle, starting from the receiving coil located under the vehicle to the battery of the vehicle. The second one is located outside the vehicle, starting from the utility AC power source until the transmitting coil.

The SAE J2954 standard [19] proposes three possibilities for the transmitting coil position: above the ground surface, flush with the ground surface, or buried. Moreover, the suggested maximum permissible protrusion above the surface of the ground is 70 mm. This distance can be more or less than the value stated above depending on the local installation rules. For now, the transmitting coil above the ground is the case adopted here. Additionally, to classify the WPT systems based on the estimated maximum ground clearance, three Z-classes are defined: Z1 = 100–150 mm, Z2 = 140–210 mm, and Z3 = 170–250 mm.

The most prevalent WPT technologies are inductive coupling and magnetic resonant coupling. Inductive coupling is a technique commonly used in wireless charging applications. Its range of operation is limited to short distances of less than a centimeter [20]. Moreover, its performance falls dramatically when there is a misalignment between the transmitting coil and the receiving coil, even when the misalignment is only a few centimeters [21].

Magnetic resonant coupling is a technique that was developed by [4]. Its range of operation can reach longer distances, and the energy is transmitted from the transmitting coil to the receiving one with high power transfer efficiency and with minimal energy losses. Figure 2 presents a block diagram of the unidirectional magnetic resonance wireless power transfer for electric vehicle charging.

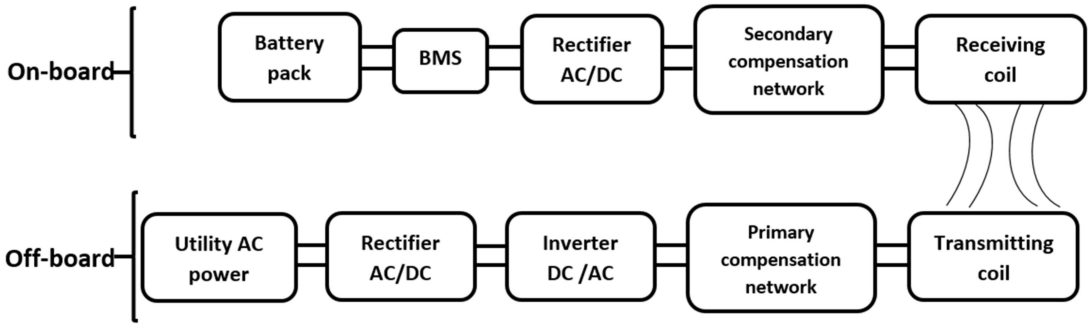

Figure 2. Unidirectional magnetic resonance wireless power transfer for electric vehicle charging.

Firstly, the utility AC power is converted to DC power by using a rectifier containing a power factor correction; then, a high-frequency inverter is used to power the compensation network and the transmitting coil. The high current flowing in the transmitting coil generates an alternating magnetic field; this magnetic field induces a voltage in the receiving coil.

Secondly, the voltage induced is rectified using an AC/DC converter, which is used to charge the battery through the battery management system (BMS). The resonance between the two compensation networks improves the transferred power and efficiency [22].

2.2. The Magnetic Resonant WPT System

In this section, the induction part of the charging system and the magnetic resonant system's equivalent circuit are discussed.

The working theory of wireless power transfer is regulated by the laws of Ampere and Faraday. Ampere's law states that a magnetic field is generated when an electric current flows through a conductor in free space. (1) indicates the relation between the magnetic field B_T created and the electric current flowing in the transmitting coil I_1, where Δl is the unit length of the conductor and N_1 is the number of turns of the transmitting coil.

$$\sum B_T \Delta l \; = \; \mu_0 I_1 N_1 \tag{1}$$

Faraday's law states that when a time-varying magnetic field relates to a conductor, it will cause a voltage to be induced in the conductor. (2) indicates the relation between the voltage e and the rate of change in magnetic flux ϕ_B, where N_2 is the number of turns of the receiving coil.

$$e \; = \; -N_2 \frac{d\phi_B}{dt} \tag{2}$$

The WPT principle is based on two coils isolated by an air gap. The transmitting coil located in the ground is powered by the AC with high frequency. As a result, a time-varying magnetic field is created according to Ampere's law. The generated magnetic field is captured by the receiving coil located below the electric vehicle and, due to Faraday's law, the magnetic field induces a voltage. The coupling coefficient k between the transmitting coil and the receiving coil plays a significant role in achieving high efficiency [2]. It is related to the mutual inductance by the following expression (3):

$$M \; = \; k\sqrt{L_1 L_2} \tag{3}$$

Figure 3 shows the equivalent circuit of the magnetic resonant WPT system model for the electric vehicle, where L_1, R_1, and C_1 are, respectively, the inductance, the resistance, and the capacitor of the primary side; L_2, R_2, and C_2 are, respectively, the inductance, the resistance, and the capacitor of the secondary side; RL is the equivalent load resistance and M is the mutual inductance between coils.

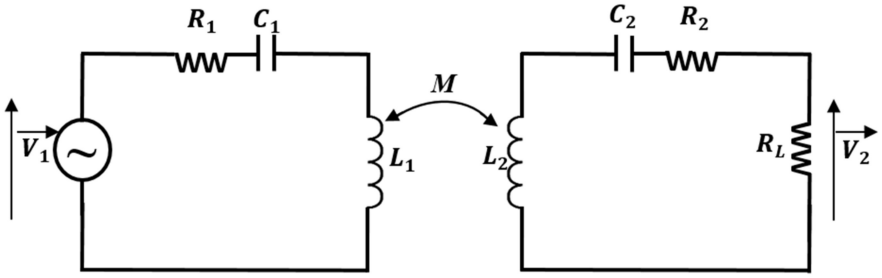

Figure 3. Equivalent circuit of magnetic resonant WPT system.

The magnetic field generated must be sufficient to connect the secondary coil; for this reason, a large current is needed. Otherwise, the inductive component must be canceled. Moreover, due to the large separation between the coils, the leakage inductance is high, as well as the proximity effect and winding resistance. Therefore, compensation capacitors are added on both the primary and secondary sides.

Different compensation topologies have been suggested in the literature to regulate the coils to work at the same frequency. These compensation networks are located between the inverter and the transmitting coil on the off-board side and between the receiving coil and the rectifier on the on-board side. The most common topologies are the four basic topologies: series–series (SS), series–parallel (SP), parallel–series (PS), and parallel–parallel (PP), as illustrated in Figure 4. Moreover, new other topologies are proposed in the literature, such as LCL compensation and LCC compensation.

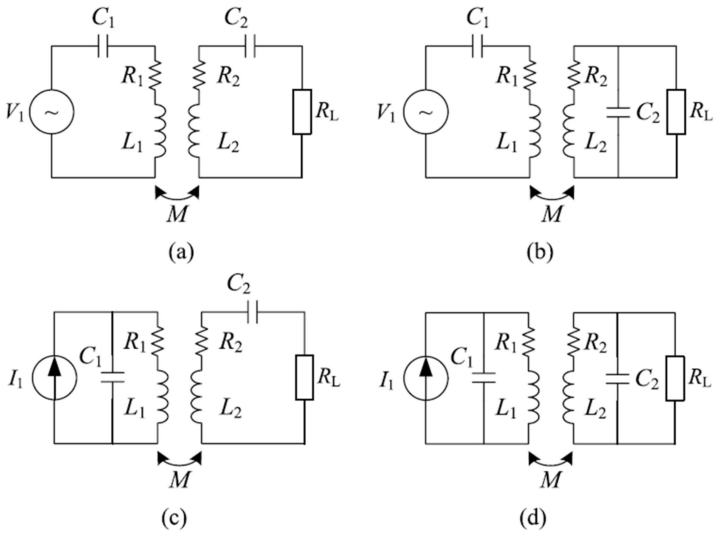

Figure 4. Four basic compensation topologies. (**a**) SS. (**b**) SP. (**c**) PS. (**d**) PP [22].

The SS topology is the only one whose primary capacitance does not depend on the coupling coefficient variation [8,23]. Moreover, at low mutual inductance, it achieves a high and stable transfer efficiency, making this topology the best choice for use with variable load conditions [24].

The calculated capacitors for the SS compensation technology are given by (4) and (5):

$$C_1 = \frac{1}{W^2 L_1} \tag{4}$$

$$C_2 = \frac{1}{W^2 L_2} \tag{5}$$

The present analysis reveals the relationship between the efficiency η and the mutual inductance M. The voltage equations of the transmitter and receiver sections can be expressed as:

$$V_1 = Z_{T1} I_1 - jwMI_2 \quad (6)$$

$$jwMI_1 = Z_{T2} I_2 \quad (7)$$

where Z_{T1} and Z_{T2} are the transmitter and receiver coil impedances, respectively, which can be expressed as:

$$Z_{T1} = \frac{1}{jwC_1} + R_1 + jwL_1 \quad (8)$$

$$Z_{T2} = \frac{1}{jwC_2} + R_2 + R_L + jwL_2 \quad (9)$$

When the system reaches the resonance frequency, and according to (4)–(6), the voltage V_1 and the current circulating in the second section I_2 are rewritten as:

$$V_1 = R_1 I_1 - jwMI_2 \quad (10)$$

$$I_2 = \frac{jwM}{R_2 + R_L} \times I_1 \quad (11)$$

The input power delivered by the voltage source P_{in} and the output power of the load P_{out} are:

$$P_{in} = V_1 I_I = \frac{R_1 \times (R_2 + R_L) + (wM)^2}{R_2 + R_L} \times {I_1}^2 \quad (12)$$

$$P_{out} = R_L {I_2}^2 = R_L \times \frac{w^2 M^2 {I_1}^2}{(R_2 + R_L)^2} \quad (13)$$

The power transfer efficiency η is then:

$$\eta = \frac{P_{out}}{P_{in}} = \frac{R_L \times (wM)^2}{(R_2 + R_L) \times [R_1 \times (R_L + R_2) + (wM)^2]} \quad (14)$$

If we consider the following condition, $R_L \gg R_2$, the efficiency is rewritten as:

$$\eta \approx \frac{1}{1 + \frac{R_1 R_L}{(wM)^2}} \quad (15)$$

Consequently, the high frequency and the large mutual inductance imply high efficiency.

3. Impacts of Coil Parameters and Coil Position on the WPT System Performance

In WPT systems for EV applications, the design of the coils used for transferring and receiving the energy must be optimized to improve the system performance. Therefore, it is essential to study what has the most impact on the coupling and efficiency of coils.

The coupling coefficient, the mutual inductance, and the coil self-inductance are the key factors in ensuring high coupling between coils. They are impacted by the coil-to-coil relative position, the addition of materials, and the coil structural parameters.

The analysis of these factors by calculation has limitations; the finite element analysis (FEA) method is the best way to execute these calculations.

The finite element method (FEM) is a numerical method based on determining approximate solutions. The main aspect of this method is to subdivide a complex problem into small pieces to generate a system of simple equations. The solutions of these equations are combined to reach the final solution.

Ansys Maxwell is a powerful finite element analysis (FEA) software program that offers many solvers to evaluate the electromagnetic component design. The system is subdivided into elements according to the mesh (a three-dimensional grid that defines

the elements). The mesh can define elements of uniform size and shape or elements of different shapes and sizes in different parts of the domain.

The boundary conditions in the Ansys Maxwell software determine the magnetic field behavior at the interfaces or the edges of the problem region. For the wireless power transfer system, the boundary conditions in the eddy current solver are determined by the air region and/or box whereby the four terminals of two coils touch the face of the boundary. Accordingly, the default parameters can be explained as follows (Table 1):

- Polygon segment: number of cross-section polygon segments;
- Polygon radius: outer radius of cross-section polygon;
- Start helix radius: start radius from polygon center to helix center, which means the radius of the first turn of the coil;
- Radius change: the distance between consecutive turns of the coil;
- Pitch: the height of the coil in the z-direction;
- Turns: the number of turns of the coil;
- Segment per turn: number of segments per turn.

Table 1. Default parameters for the model.

Coil Material	Polygon Segment	Polygon Radius	Start Helix Radius	Radius Change	Winding Number of Turns	Segment per Turn	Pitch
copper	4	1 mm	20 mm	2.05 mm	10	36	0

In this section, a reference coil model is modeled using Ansys Maxwell software to study the system.

3.1. The Two-Coil Vertical Position

The coil-to-coil relative position is a crucial factor that impacts the system coupling. The variation in the vertical distance between the coils affects positively or negatively the coupling. This section clarifies the effect of varying the vertical distance between the coils on the coil's main characteristics. The analysis covers the coupling coefficient and the mutual inductance between the transmitting and receiving coils.

A reference rectangular model is chosen. It is modeled using Ansys Maxwell software; see Figure 5. The vertical distance between the transmitting and receiving coil depends on the vehicle type and its ground clearance. It differs from one vehicle to another.

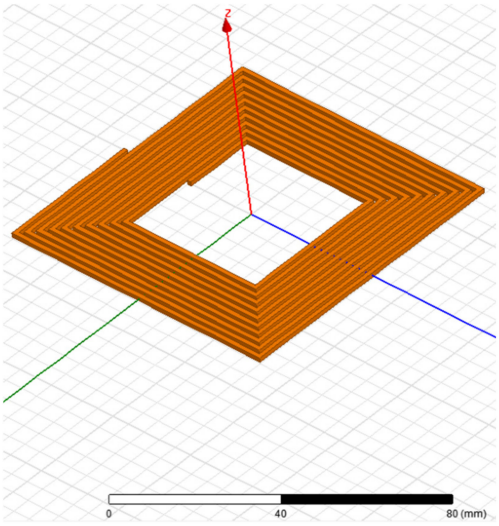

Figure 5. Reference rectangular coil model.

The gap is the vertical distance between the upper extremity of the transmitting coil and the lower extremity of the receiving coil.

In this study, to simplify the system analysis, the WPT consists of two identical rectangular coils. Figure 6 represents the three cases of rectangular coil model for gap = 100 mm.

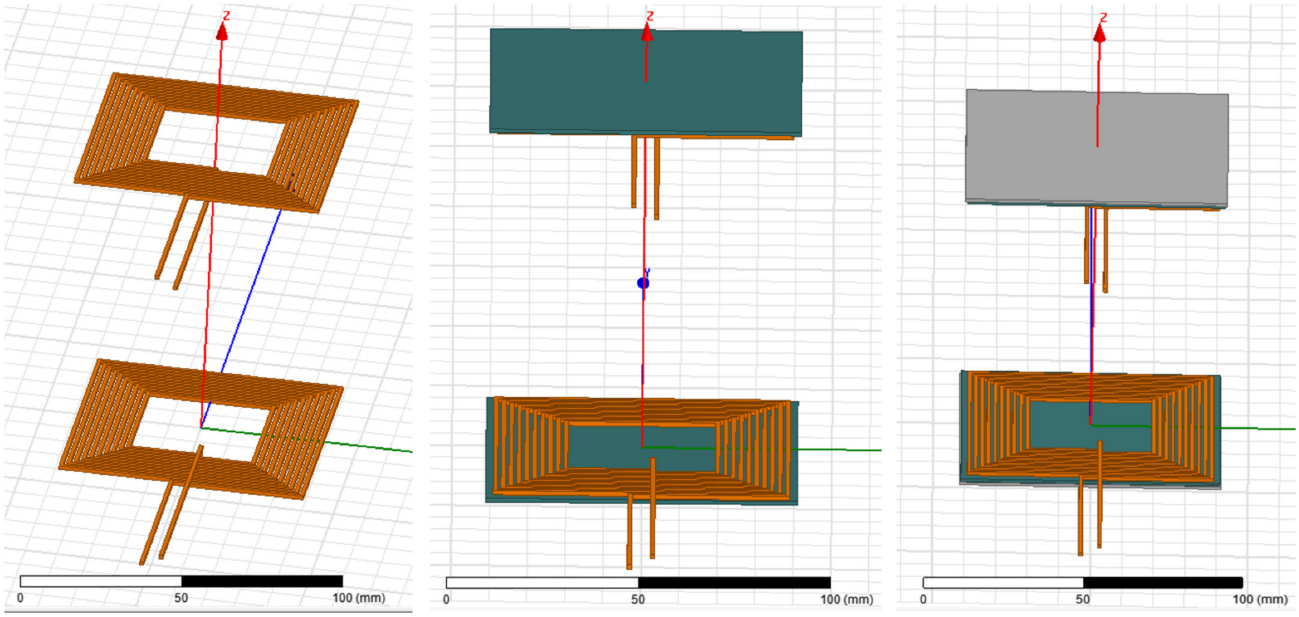

(**a**) (**b**) (**c**)

Figure 6. Rectangular coil model for gap = 100 mm: (**a**) coreless model, (**b**) model with ferrite, (**c**) model with ferrite and aluminum.

The simulation of the coreless model (Figure 6a) was carried out using Ansys Maxwell software by varying the z-distance from 50 to 300 mm.

The overall measurement results of coupling coefficient and mutual inductance for the gap variation (50–300 mm) are summarized in Table 2 and Figure 7.

The simulations indicate that the value of coefficient coupling and the mutual inductance decrease as the vertical distance between the transmitting and receiving coil increases. This implies that low power is transferred to the output as the distance increases. This type of system is referred to as a loosely coupled WPT system because the coupling coefficient between the transmitting coil TX and receiving coil RX coil is less than 0.2 [25].

The coreless transformer represents many advantages in terms of price and weight. However, the low efficiency and the decrease in system performance due to the higher core loss [26] limit its application in electric vehicle charging. Hence, specific materials are usually added to the system to improve its efficiency.

Table 2. Simulation results of rectangular coreless coil model.

Gap (mm)	Coupling Coefficient	Mutual Inductance (nH)
50	0.068109	556.24340
100	0.009552	78.193680
150	0.001664	13.567360
200	0.000319	2.609366
250	0.000054	0.427079
300	0.000000	0.000000

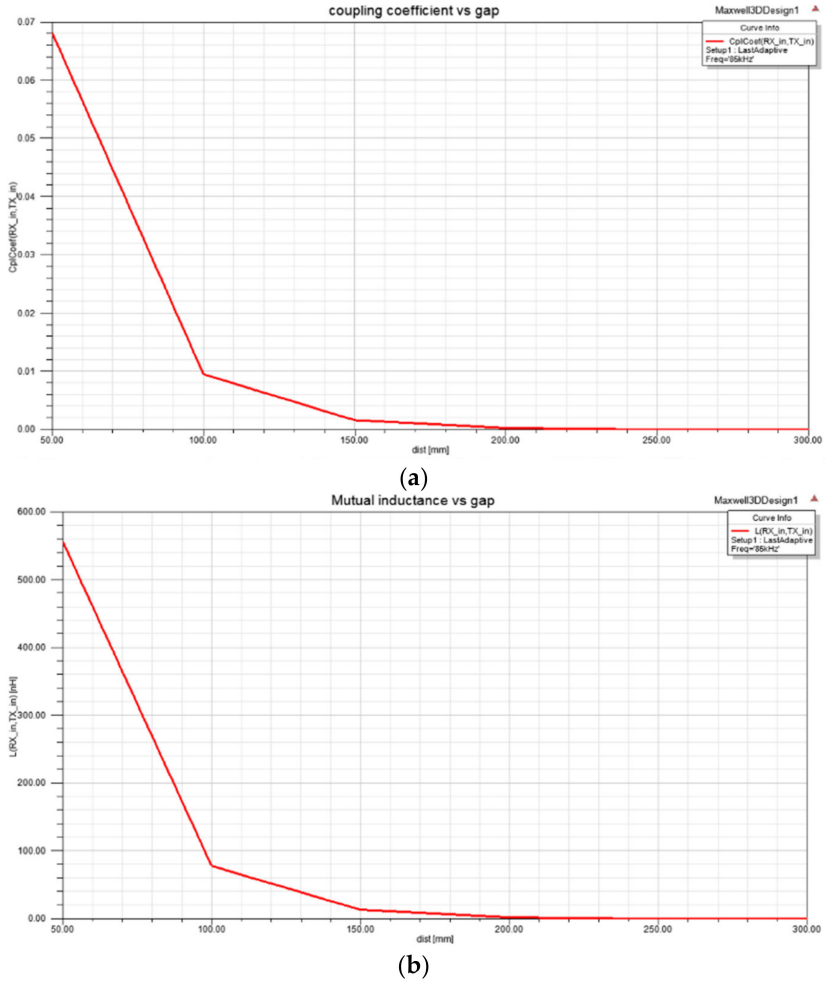

Figure 7. Rectangular coreless model: (**a**) coupling coefficient versus the gap variation, (**b**) mutual inductance versus the gap variation.

3.2. The Introduction of Ferrite and Aluminum to the Coil System

Several studies have been carried out to enhance the weak coupling resulting from the two coils inductively coupled; one of the efficient methods is the integration of new materials into the system. These materials should not affect the electrical performance of the system. The main objective is to enhance the coupling between the coils and minimize the leakage flux by guiding the flux from the transmitter coil to the receiver coil.

The relative permeability of ferrite is high and can reduce the reluctance path [26]. Moreover, according to [27], the hysteresis loop of Mn-Zn ferrite is narrow, which helps to minimize hysteresis loss. As a result, ferrite bars or plates are often used to guide magnetic flux and provide magnetic shielding.

A simple analysis is performed using a ferrite plate to analyze the coupling concerning the gap variation. The same rectangular shape is chosen. Figure 6b illustrates the rectangular coil with ferrite for gap = 100 cm.

Table 3 and Figure 8 depict the simulation results of the coupling coefficient and mutual inductance for the gap variation (50 to 300 mm).

The result shows that the coupling coefficient and the mutual inductance values decrease as the z-distance increases. Moreover, the values have been greatly increased compared to the coreless results. The ferrite is dedicated to providing an alternative path for the lines of the magnetic flux and changing its usual path [28].

Table 3. Simulation results of rectangular coil model with ferrite.

Gap (mm)	Coupling Coefficient	Mutual Inductance (µH)
50	0.101212	1.452432
100	0.013244	0.189907
150	0.002227	0.031972
200	0.000425	0.006089
250	0.000081	0.001156
300	0.000012	0.000169

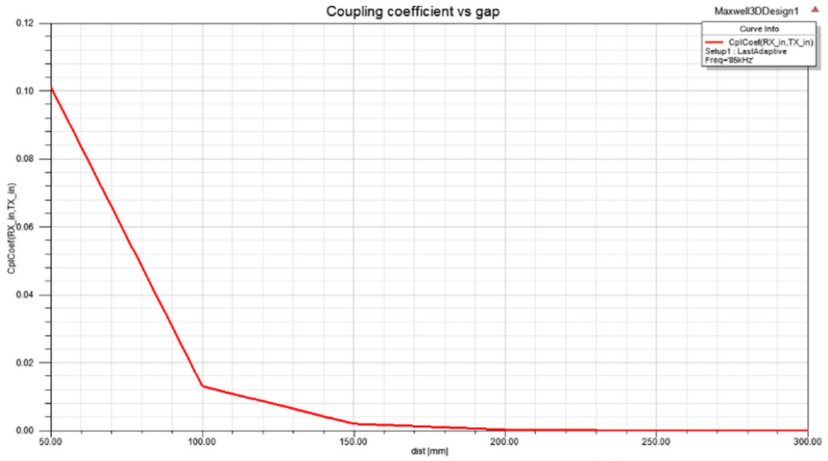

(**a**)

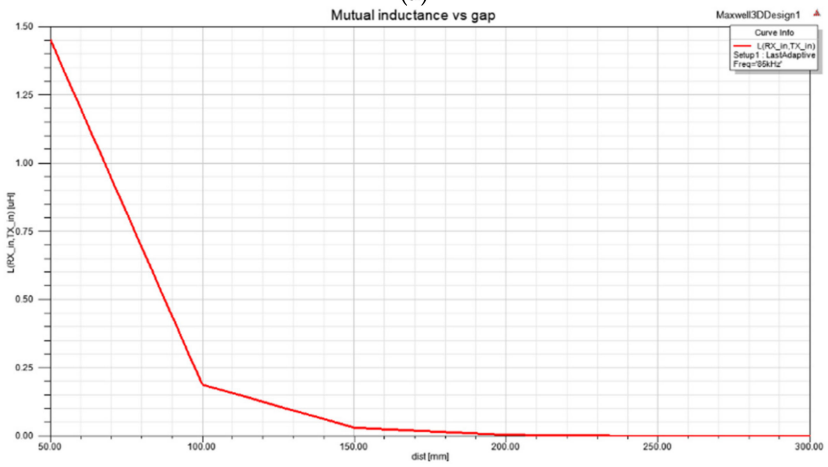

(**b**)

Figure 8. Rectangular coil model with ferrite: (**a**) coupling coefficient versus the gap variation, (**b**) mutual inductance versus the gap variation.

Otherwise, among the advantages of using ferrite, it can reduce the serious risks for the user's health. Thereby, it is considered magnetic shielding. However, this type of shielding may not be sufficient to protect users and respect the guidance of the ICNIRP standard [29].

An aluminum plate is added to the system to analyze its influence on the coupling. Figure 6c shows the rectangular coil with ferrite and aluminum for gap = 100 mm.

The simulation results of the coupling coefficient and the mutual inductance are summarized in Table 4 and Figure 9.

Table 4. Simulation results of rectangular coil model with ferrite and aluminum.

Gap (mm)	Coupling Coefficient	Mutual Inductance (μH)
50	0.100854	1.448542
100	0.013164	0.188223
150	0.002217	0.031680
200	0.000423	0.006059
250	0.000081	0.001157
300	0.000013	0.000179

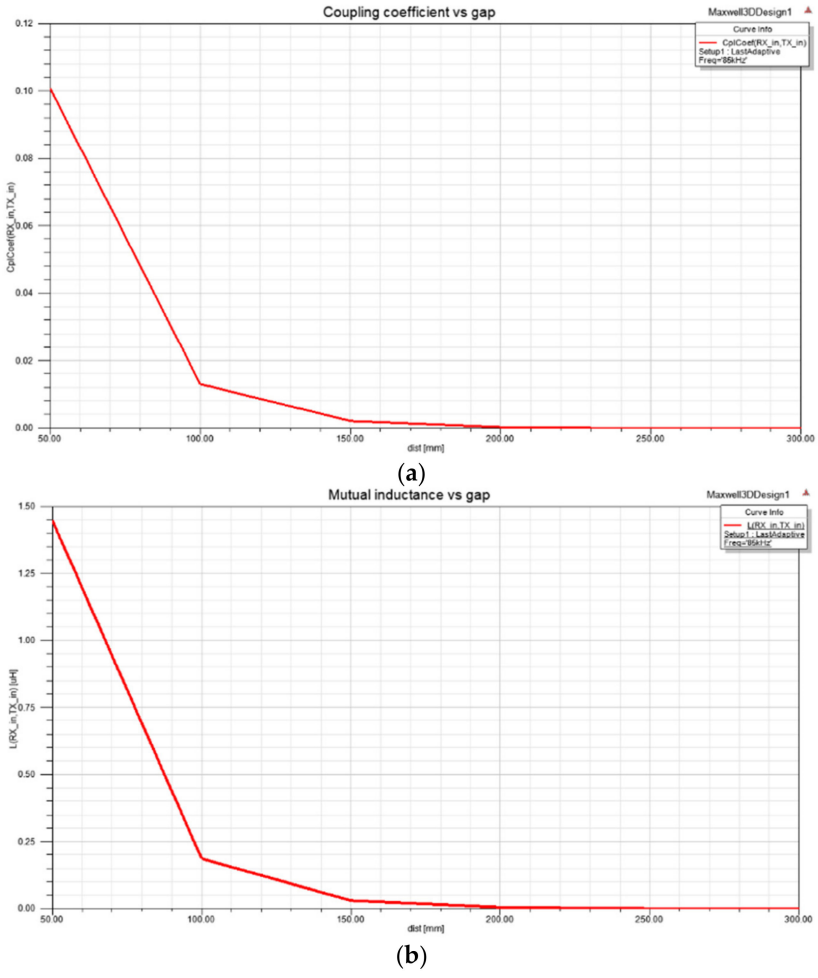

Figure 9. Rectangular coil model with ferrite and aluminum: (**a**) coupling coefficient versus the gap variation, (**b**) mutual inductance versus the gap variation.

It can be concluded that the coil with ferrite represents the highest coupling coefficient value among all three cases (case 1: coreless coil, case 2: a coil with ferrite, case 3: a coil with ferrite and aluminum). This result is due to the ferrite, which collects the flux and guides it along another path.

The introduction of aluminum to the rectangular coil with ferrite reduces marginally the coupling coefficient value while remaining relatively high [2]. According to [3,30], it is possible to reduce the variation in circuit parameters while maintaining the shielding effect if the ferrite is positioned between the coil and aluminum plate and the thickness of the aluminum is greater than the skin depth.

There are several types of shielding in the literature [3,31,32]. The working principle of conductive shielding can be explained as follows: the magnetic field generated by the coils induces eddy currents in the aluminum shield. These eddy currents in turn create an opposing magnetic field to attenuate or even cancel out the incident magnetic field [16,31].

Hence, by adding the ferrite and aluminum to the system, the characteristics are also merged. This means that the coupling is increased compared to case 1 and the magnetic field is better shielded compared to case 2.

The limitation and guidance of magnetic flux lines not only lead to a decrease in the leakage magnetic field but also an increase in coupling coefficient and mutual inductance.

In summary, both ferrite and aluminum are necessary to ensure good coupling and better shielding to meet the ICNIRP guidelines (ICNIRP).

3.3. Coil Main Parameters

The coupling coefficient, self-inductance, and the mutual inductance of two coils are considered as crucial factors determined by coil parameters that affect the system performance. Therefore, improvement of the coil parameters is a suitable means of enhancing the system coupling. The variation in coil parameters affects the system coupling by varying either the number of turns or the inner radius or other parameters. In this section, the impact of varying these parameters on the system coupling is analyzed. The simulations were performed by modeling a circular coil using Ansys Maxwell software (Figure 10). Accordingly, the model characteristics can be explained as follows (Table 5):

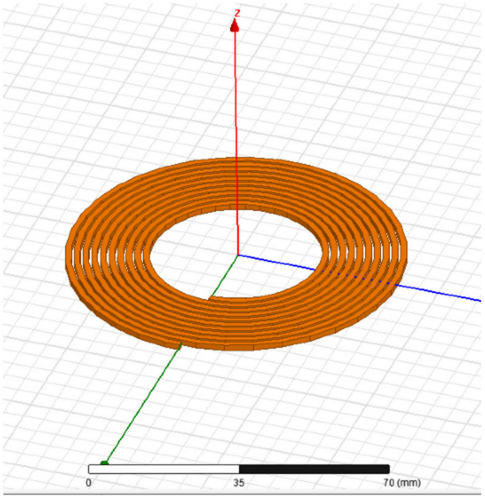

Figure 10. Reference circular coil model.

Table 5. Circular coil model characteristics.

Coil Material	Winding Number of Turns	Winding Diameter	Pitch
Copper	10	Outer 80 mm Inner 40 mm	0

3.3.1. The Coil Inner Radius

In this analysis, the inner radius of the transmitting coil is kept constant, $R_{TX} = 20$ mm, and that of the receiving coil R_{RX} is changed from 10 to 40 mm. Figure 11 illustrates an example of two cases: (a) $R_{RX} = 10$ mm and (b) $R_{RX} = 40$ mm. The number of turns for both coils is equal to $N_{RX} = N_{TX} = 20$ mm. The simulation results of the coupling coefficient regarding the receiving coil inner radius variation for gap = 100 mm are illustrated in Table 6 and Figures 12 and 13.

The inner radius of the receiving coil in the first image is equal to 10 mm and the inner radius of the receiving coil in the second image is equal to 40 mm.

The same procedure is applied to the transmitting coil. The inner radius of the receiving coil is constant and we change that of the transmitting coil. The other parameters are kept the same.

Figure 14 illustrates an example of two cases: (a) $R_{TX} = 10$ mm and (b) $R_{TX} = 40$ mm.

The simulation result of the coupling coefficient regarding the transmitting coil inner radius variation for gap = 100 mm is shown in Table 7 and Figures 15 and 16.

Table 6. Simulation results of circular coil model—R_{RX} variation.

R_{RX}	10	15	20	25	30	35	40
Coupling coefficient	0.005816	0.007161	0.008412	0.009585	0.010463	0.011186	0.011684
Mutual inductance (nH)	30.424290	44.193950	59.199180	74.752330	89.813510	103.64980	115.51350
L1 (µH)	6.780342	6.779160	6.785520	6.791254	6.794025	6.793827	6.798295
L2 (µH)	4.036471	5.617566	7.298441	9.050857	10.844590	12.637880	14.37701

Table 7. Simulation results of circular coil model—R_{TX} variation.

R_{TX}	10	15	20	25	30	35	40
Coupling coefficient	0.005711	0.007095	0.008412	0.009605	0.010627	0.011418	0.011990
Mutual inductance (nH)	30.39108	44.18762	59.19918	74.67751	89.77743	103.5061	115.4117
L1 (µH)	3.874879	5.307868	6.785520	8.276253	9.770129	11.25197	12.68043
L2 (µH)	7.308522	7.308452	7.298441	7.303525	7.305497	7.302940	7.307154

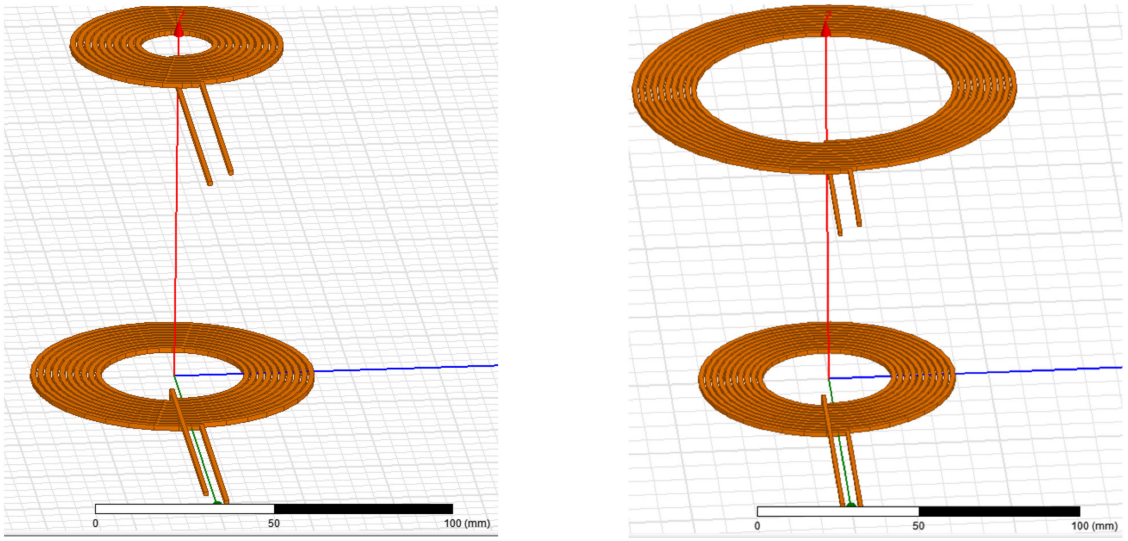

(**a**) (**b**)

Figure 11. Coreless coil models with constant R_{TX}: (**a**) R_{RX} = 10 mm, (**b**) R_{RX} = 40 mm for gap = 100 mm.

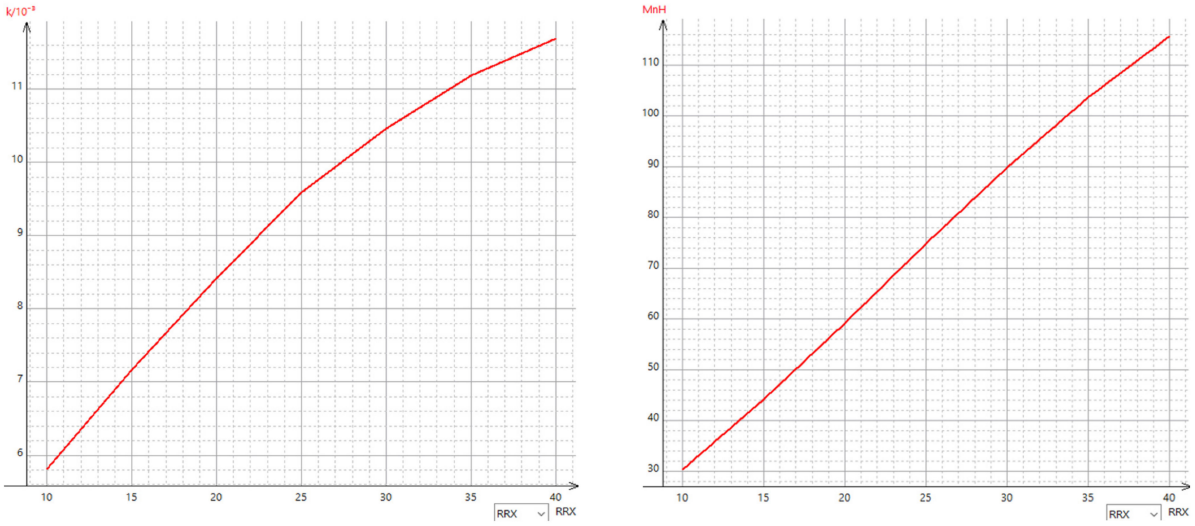

Figure 12. R_{RX} variation simulation results of circular coil model: k in the function of R_{RX} and M in the function of R_{RX}.

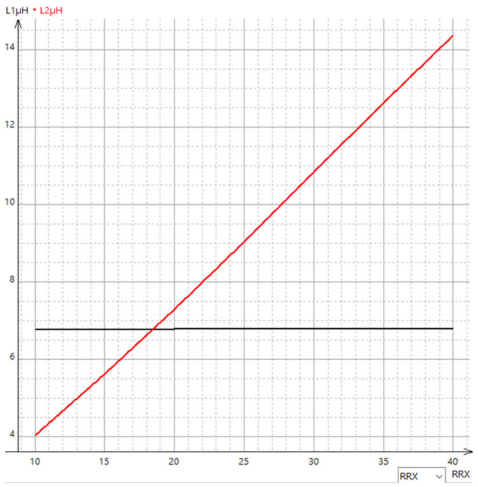

Figure 13. R_{RX} variation simulation results of circular coil model: L_1 in the function of R_{RX}, L_2 in the function of R_{RX}.

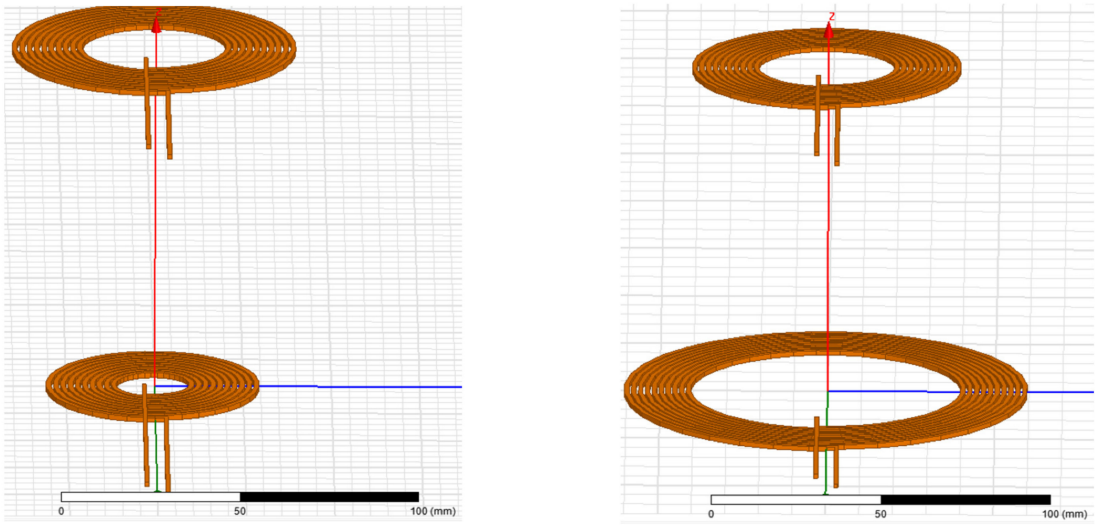

(**a**) (**b**)

Figure 14. Coreless coil models with constant R_{TX}: (**a**) R_{RX} = 10 mm, (**b**) R_{RX} = 40 mm for gap = 100 mm.

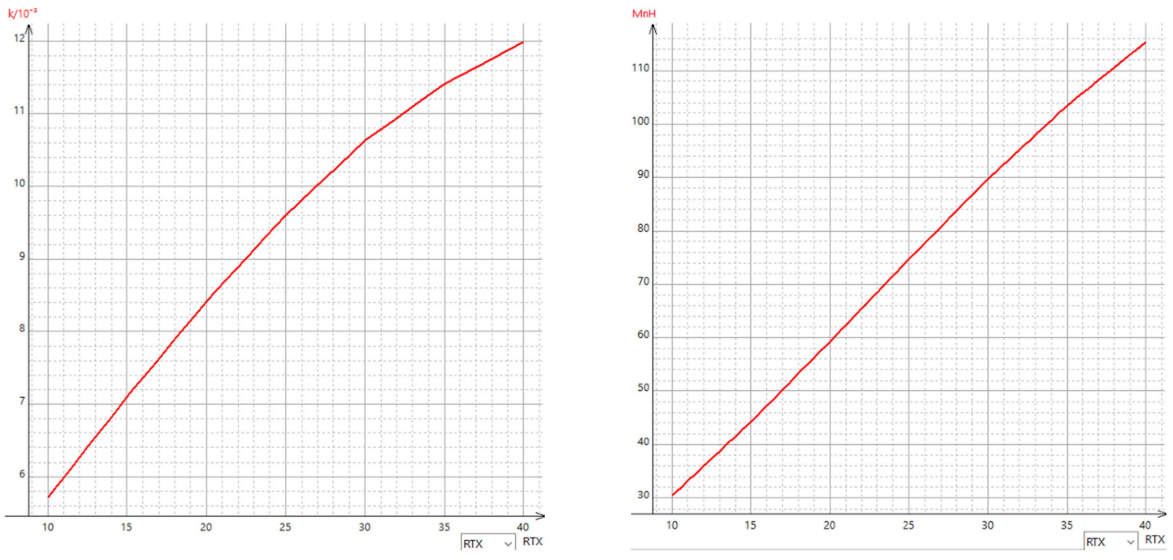

Figure 15. R_{TX} variation simulation results of circular coil model: k in the function of R_{TX}, M in the function of R_{TX}.

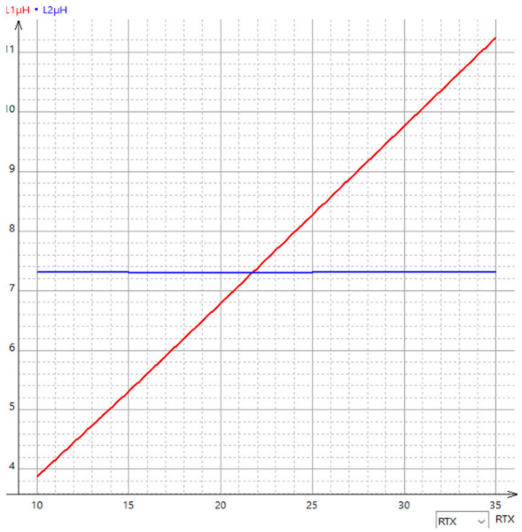

Figure 16. R_{TX} variation simulation results of circular coil model: L_1 in the function of R_{TX}, L_2 in the function of R_{TX}.

The results indicate that the coil inner radius variation has a significant effect on the system coupling.

Thus, increasing the inner radius of the transmitting or the receiving coil while keeping the other parameters constant enhances the value of the coupling coefficient. The same results are found for the mutual inductance. Therefore, although the two coils present different functions (transmitting and receiving the energy), their attitude towards the self-inductance is the same. Note also that the coil whose inner radius changes its self-inductance also changes and remains constant if no other parameters are modified, i.e., the inductance follows the variation in the inner radius.

Figure 17 presents a cross-sectional view of a flat circular coil.

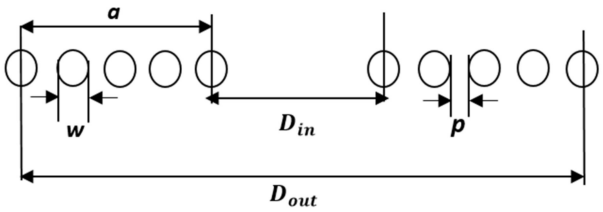

Figure 17. A cross-sectional view of the flat circular coil.

Here, D_{out} is the outer diameter, D_{in} is the inner diameter, w is the wire diameter, and p is the spacing between the adjacent wire. From the figure, we can deduce the relation between coil radius R and coil inner radius R_{in} as:

$$R = R_{in} + a = \frac{D_{in}}{2} + a \tag{16}$$

If a is a constant, this means that the spacing between adjacent wire p, the wire diameter w, and the coil number of turns N is constant, and any increase in the inner radius R_{in} leads to an increase in the coil radius. Therefore, any augmentation in the coil inner radius or the radius of the coil increases the inductance of the coil. These results are consistent with those found in [33], where the inductance is a monotonic function of the coil radius.

However, because the space taken up by the receiving coil in the vehicle chassis is limited, the coil cannot be completely increased, even if the large inner radius gives good coupling results. This space differs from one vehicle to another; therefore, if the pad design is dedicated to a specific vehicle, the inner radius must be large, depending on the spacing

offered. On the other hand, if the pad is designed to be suitable for different types of vehicles, its parameters, including the inner radius, must follow dedicated standards.

3.3.2. The Coil Number of Turns

In this analysis, the number of turns of the transmitting coil is preserved constantly N_{TX} = 10 and we change that of the receiving coil from 5 to 16. The inner radius for both coils is equal to $R_{RX} = R_{TX}$ = 20 mm. The simulation results of the coupling coefficient regarding the receiving coil number of turns for gap = 100 mm are illustrated in Table 8 and Figures 18 and 19.

Table 8. Simulation results of circular coil model—number of turns N_{RX} variation.

Number of Turns N_{RX}	5	7	10	13	16
Coupling coefficient	0.005873	0.006941	0.008412	0.009744	0.010916
Mutual inductance (nH)	21.589390	34.704880	59.199180	89.343810	123.96730
L1 (µH)	6.784625	6.792092	6.785520	6.787126	6.774364
L2 (µH)	1.991499	3.680638	7.298441	12.386530	19.039200

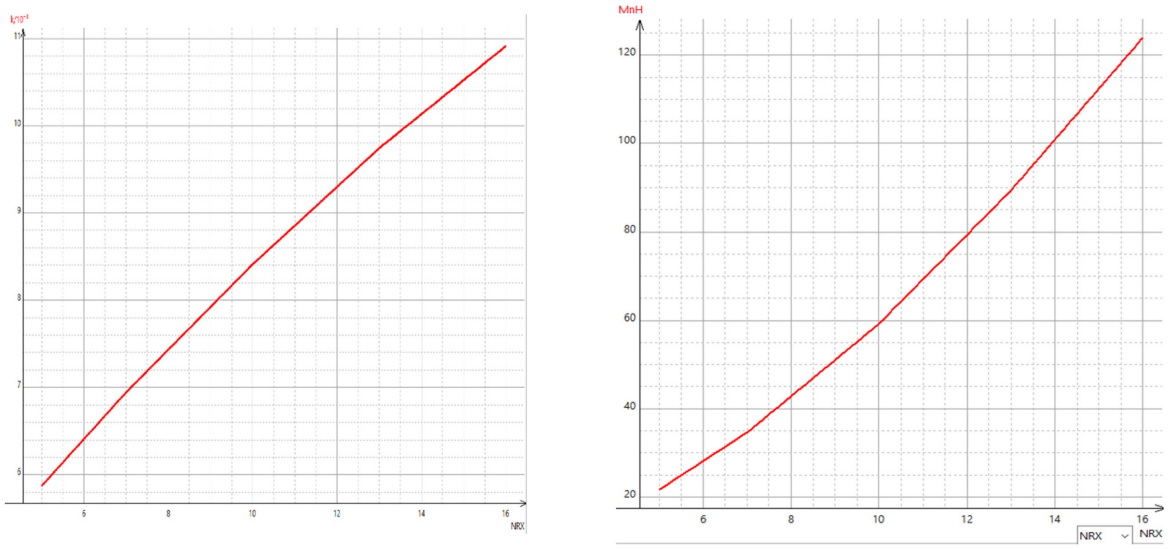

Figure 18. Number of turns simulation results of circular coil model: k in the function of N_{RX}, M in the function of N_{RX}.

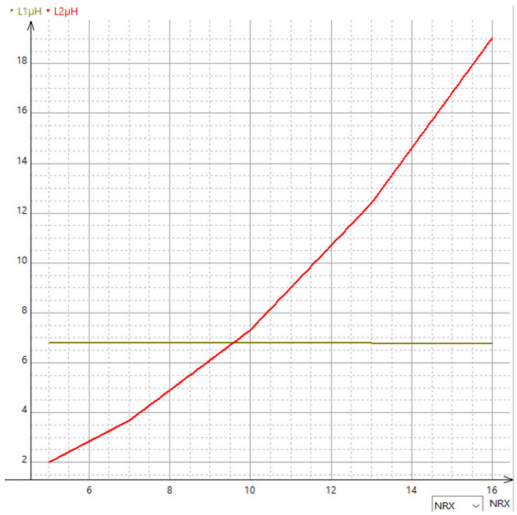

Figure 19. Number of turns simulation results of circular coil model: L_1 in the function of N_{RX}, L_2 in the function of N_{RX}.

The same procedure is applied to the transmitting coil. The inner radius of the receiving coil is constant and that of the transmitting coil is changed. The other parameters are kept the same.

The simulation result of the coupling coefficient regarding the transmitting coil number of turns variation for gap = 100 mm is shown in Table 9 and Figures 20 and 21.

Table 9. Simulation results of circular coil model—number of turns N_{TX} variation.

Number of Turns N_{TX}	5	7	10	13	16
Coupling coefficient	0.006331	0.006856	0.008412	0.009836	0.011129
Mutual inductance (nH)	27.788710	34.660960	59.199180	89.228940	123.91930
L1 (µH)	2.639758	3.498766	6.785520	11.276280	16.990020
L2 (µH)	7.299475	7.304379	7.298441	7.298372	7.296844

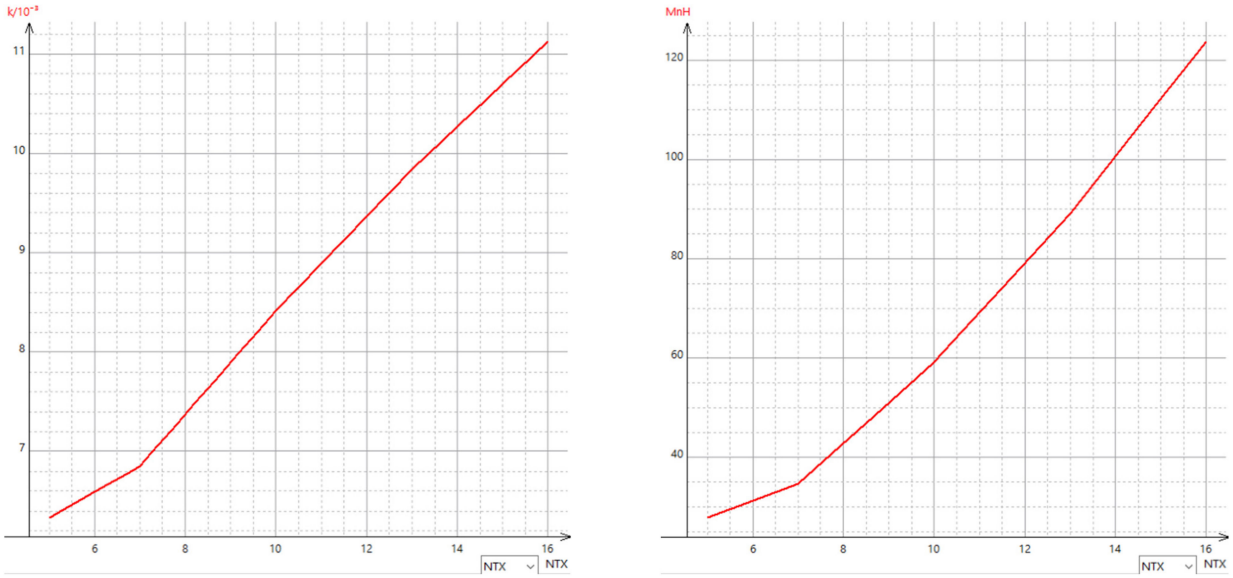

Figure 20. Number of turns simulation results of circular coil model: k in the function of N_{TX}, M in the function of N_{TX}.

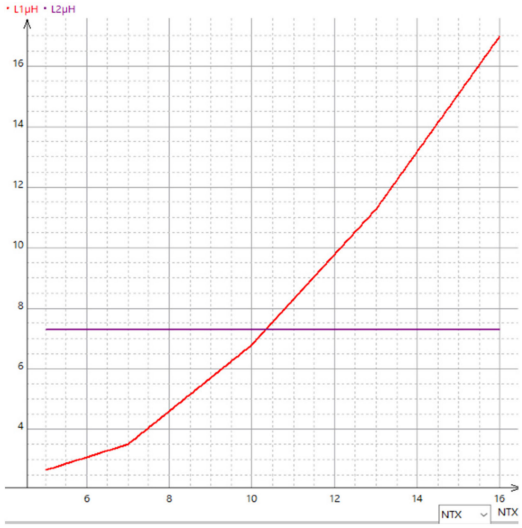

Figure 21. Number of turns simulation results of circular coil model: L_1 in the function of N_{TX}, L_2 in the function of N_{TX}.

The results indicate that the coil number of turns affects the system coupling. Increasing the number of turns of the transmitting and receiving coils while keeping the other

parameters constant enhances the coupling coefficient and the mutual inductance values. Furthermore, for the coil whose number of turns increases, its inductance also increases and remains constant if no parameters are modified, i.e., the inductance follows the variation in the number of turns.

Moreover, if the number of turns increases, the outer diameter increases effectively by default. Here, the concept of misalignment is introduced. The misalignment is a major factor that we should take into consideration while designing the coils. According to SAE J2954 (SAE), the lateral misalignment tolerance among the x-axis (vehicle movement) is ± 100 mm, so if we consider that the outer diameter of the transmitting coil is named D_{TXout}, the diameter of the receiving coil must then be D_{RXout}:

$$D_{RXout} = D_{TXout} - 200 \text{ mm} \tag{17}$$

This expression ensures that the misalignment is reduced according to the misalignment tolerance.

Therefore, increasing the number of turns of the coil remains an effective method to improve the inductance of the coil and to improve the coupling coefficient in the wireless power transfer system, taking into account the notion of misalignment.

It can be concluded that the coupling coefficient, mutual inductance, and coil inductance depend on the coil parameters and the relative position of the coils. Effectively, the study results reveal that the optimized design of the coil inner radius and number of turns is beneficial in improving the coupling and mutual inductance abilities.

4. Comparison of Three Coil Shapes for EV Charging Application

4.1. The Three Coil Shapes' Comparison

In this section, three coil shapes are presented: circular, rectangular, and hexagonal (Figure 22). The main objective is to compare the coupling coefficient, the mutual inductance, and the coil inductance for the three coil shapes. The comparison is set for air gaps of z = 50 mm up to z = 300 mm with steps of 50 mm and for zero misalignments ($d_x = d_y = 0$).

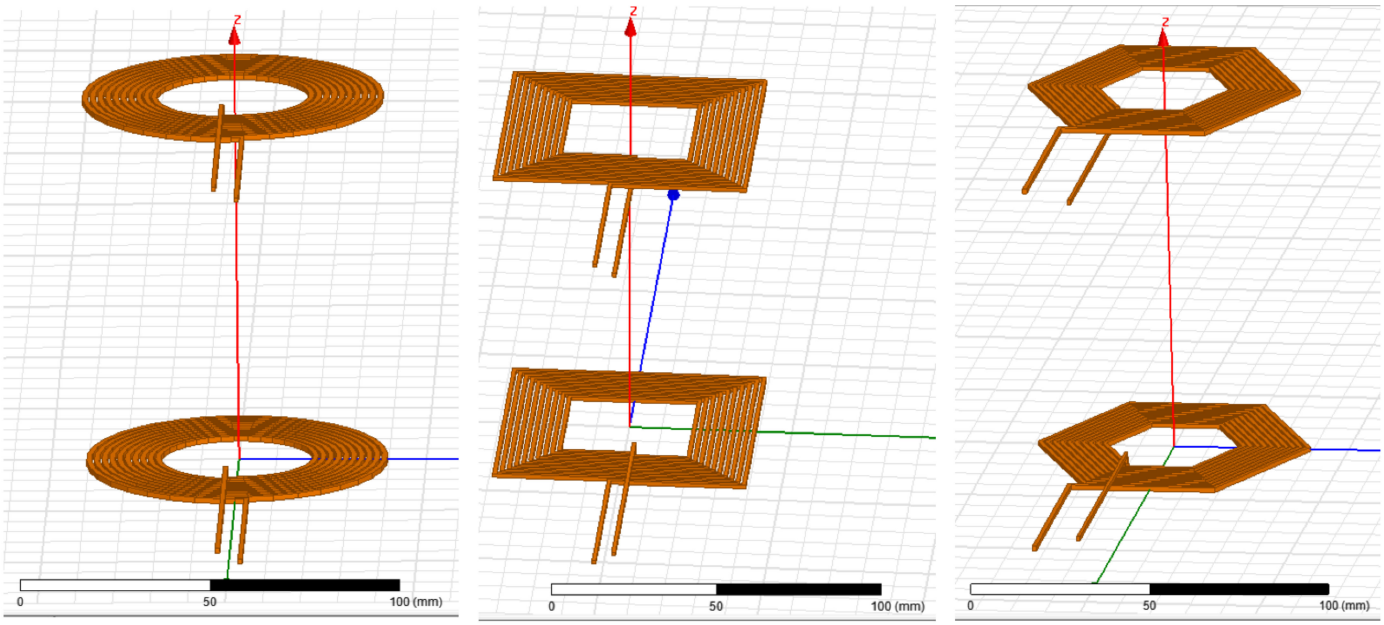

(**a**) (**b**) (**c**)

Figure 22. The three cases: (**a**) circular coreless model, (**b**) rectangular coreless model, (**c**) hexagonal coreless model.

For a reliable and reasonable comparison, the three coils' main parameters are designed to be equal, namely the number of turns, the inner diameter, the outer diameter, pitch, and the spacing between the adjacent wire. The dimensions of the coils are given in Table 10.

Table 10. The three coil main parameters.

Inner Diameter	Outer Diameter	Number of Turns	Pitch	The Spacing between Adjacent Wires	Frequency	Initial Current
40 mm	80 mm	10	0	0.7 mm	85 kHz	25 A

The simulations of the three coils topologies are performed using Ansys Maxwell software and compared regarding the coupling coefficient, mutual inductance, and coil inductance. The simulations are conducted using an eddy current solution with a frequency of 85 kHz and a constant current of the transmitting coil. In addition, the direction of the current in the internal winding is opposite to that of the external winding and the coil size remains the same for all simulations.

The simulation results of the three geometries for the three cases—case 1: circular coil, case 2: rectangular coil, case 3: hexagonal—are presented in Tables 11 and 12.

Here, the parameters used in the following tables are defined as:

- k_c, k_r, and k_h are the coupling coefficient of circular, rectangular, and hexagonal coils, respectively;
- M_c, M_r, and M_h are the mutual inductance of circular, rectangular, and hexagonal coils, respectively;
- L_{1c}, L_{1r}, and L_{1h} are the inductance of circular, rectangular, and hexagonal transmitting coils, respectively;
- L_{2c}, L_{2r}, and L_{2h} are the inductance of circular, rectangular, and hexagonal receiving coils, respectively.

Table 11. The simulation results (k, M) of the three geometries: case 1, case 2, and case 3.

Gap (mm)	k_c	M_c	k_r	M_r	k_h	M_h
Case 1						
50	0.063451	445.95400	0.068109	556.24340	0.057182	397.82520
100	0.008412	59.199180	0.009552	78.193680	0.007409	51.661350
150	0.001441	10.143700	0.001664	13.567360	0.001265	8.812501
200	0.000280	1.969708	0.000319	2.609366	0.000246	1.712719
250	0.000049	0.331442	0.000054	0.427079	0.000043	0.290551
300	0.000004	0.017259	0.000000	0.000000	0.000003	0.001513
Case 2						
50	0.087542	1.052032	0.101212	1.452432	0.086132	1.084909
100	0.010632	0.127913	0.013244	0.189907	0.010165	0.127640
150	0.001755	0.021099	0.002227	0.031972	0.001658	0.020777
200	0.000339	0.004080	0.000425	0.006089	0.000312	0.003920
250	0.000068	0.000811	0.000081	0.001156	0.000059	0.000740
300	0.000011	0.000125	0.000012	0.000169	0.000009	0.000103
Case 3						
50	0.064083	690.79670	0.100854	1.448542	0.085573	1.072621
100	0.006945	75.680240	0.013164	0.188223	0.010104	0.126605
150	0.001097	11.840260	0.002217	0.031680	0.001645	0.020617
200	0.000211	2.298739	0.000423	0.006059	0.000310	0.003883
250	0.000045	0.480430	0.000081	0.001157	0.000059	0.000734
300	0.000010	0.105318	0.000013	0.000179	0.000009	0.000110

Table 12. The simulation results (L_1, L_2) of the three geometries: case 1, case 2, and case 3.

Gap (mm)	L_{1c}	L_{2c}	L_{1r}	L_{2r}	L_{1h}	L_{2h}
			Case 1			
50	0.064083	690.79670	0.100854	1.448542	0.085573	1.072621
100	0.006945	75.680240	0.013164	0.188223	0.010104	0.126605
150	0.001097	11.840260	0.002217	0.031680	0.001645	0.020617
200	0.000211	2.298739	0.000423	0.006059	0.000310	0.003883
250	0.000045	0.480430	0.000081	0.001157	0.000059	0.000734
300	0.000010	0.105318	0.000013	0.000179	0.000009	0.000110
			Case 2			
50	11.947130	12.088330	14.298380	14.402650	12.562350	12.629550
100	11.950400	12.110930	14.266830	14.412460	12.513560	12.600940
150	11.957580	12.091200	14.256900	14.457540	12.474230	12.589890
200	11.926060	12.117880	14.263890	14.402940	12.515170	12.633200
250	11.941690	11.923480	14.226600	14.216720	12.504320	12.497870
300	11.808270	10.570560	14.300310	12.999270	12.510930	11.797060
			Case 3			
50	10.781420	10.777930	14.281620	14.444460	12.492290	12.577110
100	10.869160	10.925570	14.209700	14.387980	12.471550	12.590100
150	10.792140	10.799971	14.204850	14.378430	12.469870	12.593910
200	10.903430	10.917850	14.243580	14.429750	12.455440	12.570840
250	10.785930	10.783920	14.226220	14.227060	12.458240	12.445430
300	10.864260	10.687310	14.189000	13.187760	12.458490	11.860980

For the coreless case, the results show that the rectangular shape represents the greatest coupling coefficient k and mutual inductance M compared to the circular and hexagonal shapes.

The circular coil is the second shape that has a good coupling coefficient, while the coupling coefficient of the hexagonal coil is also close to this value.

The introduction of ferrite and aluminum into the coils enhances the coupling coefficient values for all shapes, as can be concluded from Section 3. Notably, the rectangular shape still presents the best values.

Moreover, the transmitting coil inductance remains unchanged when the vertical distance is varied. Effectively, there is no change in the coil parameters and the current flowing in the transmitting coil is considered constant. When the ferrite is added, the inductance improves and remains constant over all gap variation. Moreover, the introduction of aluminum into the system composed of coil and ferrite marginally reduces the inductance value, which remains notably high. In this case, the rectangular coil presents the best value of L2 compared to the circular and hexagonal, especially after adding the ferrite.

On the other hand, the rectangular and hexagonal receiving coils' inductance in the coreless case decrease with the large vertical distances (300 mm). This influence diminishes by adding ferrite and aluminum. However, the receiving circular coil inductance remains a high value basically in the large vertical distances.

These results give the advantage to the rectangular shape, with high coupling and inductance values, over other shapes for the variation in the gap under the given conditions. Other factors that can alter these results are the static or dynamic type of charging of electric vehicles and the misalignment of coils along the x and y-axis. Therefore, these coils are of different natures and are suitable for specific applications.

Several studies have been carried out to determine the coil inductance expressions, namely the modified Wheeler formula, the expression based on current sheet approximation, and the data-fitted monomial expression [34]. Thereby, the ratio between the current flowing through the coil and the magnetic flux generated represents its self-inductance [35].

Hence, the self-inductance of the coil is expressed as follows [34]:

$$L = \frac{\mu N^2 d_{avg} C_1}{2}\left(\ln\left(\frac{C_2}{\rho}\right) + C_3\rho + C_4\rho^2\right) \quad (18)$$

where μ_0 is the permeability of free space, N is the number of turns, d_{out} and d_{in} are the outer and inner diameters of the coil, $d_{avg} = \frac{d_{in}+d_{out}}{2}$ is the average diameter, $\rho = \frac{d_{out}-d_{in}}{d_{out}+d_{in}}$ is the fill factor. The coefficients C_i are layout-dependent, as illustrated in Table 13.

Table 13. Coefficients for current sheet expression.

Layout	C_1	C_2	C_3	C_4
Square	1.27	2.07	0.18	0.13
Hexagonal	1.09	2.23	0.00	0.17
Octagonal	1.07	2.29	0.00	0.19
Circle	1.00	2.46	0.00	0.20

4.2. The Nine Possibilities of the Three Shapes' Combination

There are different possible shapes for the receiving coil attached to the bottom of vehicles, the same as for the transmitting coils located at charging stations. For this, we propose in this part nine possibilities that can be encountered in wireless charging operations using the three coil shapes: circular, rectangular, and hexagonal. Each shape of the transmitting coil corresponds to the three shapes of the receiving coil. The topologies consist of air-core coils without any material to ensure equitable comparison.

To compare the nine possibilities of shaped coils, their self- and mutual inductances and coupling coefficients were calculated using FEM software.

The modeling of the different coils can be considered the same as in the section above. The 3-D models created in ANSYS Maxwell software for the nine shapes' cases can be described as follows:

Case 1: circular transmitter coil and circular receiving coil;
Case 2: circular transmitter coil and rectangular receiving coil;
Case 3: circular transmitter coil and hexagonal receiving coil;
Case 4: rectangular transmitter coil and circular receiving coil;
Case 5: rectangular transmitter coil and rectangular receiving coil;
Case 6: rectangular transmitter coil and hexagonal receiving coil;
Case 7: hexagonal transmitter coil and circular receiving coil;
Case 8: hexagonal transmitter coil and rectangular receiving coil;
Case 9: hexagonal transmitter coil and hexagonal receiving coil.

The simulation results of the coils for the nine cases are presented in Tables 14 and 15. Here, the parameters used in the following tables are defined as follows:

- k_{cc}, k_{cr}, and k_{ch} are the coupling coefficients of the combination of transmitting circular coil and receiving circular, rectangular, and hexagonal coils, respectively;
- M_{cc}, M_{cr}, and M_{ch} are the mutual inductances of the combination of transmitting circular coil and receiving circular, rectangular, and hexagonal coils, respectively;
- k_{rc}, k_{rr}, and k_{rh} are the coupling coefficients of the combination of transmitting rectangular coil and receiving circular, rectangular, and hexagonal coils, respectively;
- M_{rc}, M_{rr}, and M_{rh} are the mutual inductances of the combination of transmitting rectangular coil and receiving circular, rectangular, and hexagonal coils, respectively;
- k_{hc}, k_{hr}, and k_{hh} are the coupling coefficients of the combination of transmitting hexagonal coil and receiving circular, rectangular, and hexagonal coils, respectively;
- M_{hc}, M_{hr}, and M_{hh} are the mutual inductances of the combination of transmitting hexagonal coil and receiving circular, rectangular, and hexagonal coils, respectively;

- L_{1cc}, L_{1cr}, and L_{1ch} are the self-inductance of transmitting coils in the combination of transmitting circular coil and receiving circular, rectangular, and hexagonal coils, respectively;
- L_{2cc}, L_{2cr}, and L_{2ch} are the self-inductance of receiving coils in the combination of transmitting circular coil and receiving circular, rectangular, and hexagonal coils, respectively;
- L_{1rc}, L_{1rr}, and L_{1rh} are the self-inductance of transmitting coils in the combination of transmitting rectangular coil and receiving circular, rectangular, and hexagonal coils, respectively;
- L_{2rc}, L_{2rr}, and L_{2rh} are the self-inductance of receiving coils in the combination of transmitting rectangular coil and receiving circular, rectangular, and hexagonal coils, respectively;
- L_{1hc}, L_{1hr}, and L_{1hh} are the self-inductance of transmitting coils in the combination of transmitting hexagonal coil and receiving circular, rectangular, and hexagonal coils, respectively;
- L_{2hc}, L_{2hr}, and L_{2hh} are the self-inductance of receiving coils in the combination of transmitting hexagonal coil and receiving circular, rectangular, and hexagonal coils, respectively.

The coupling coefficient and the mutual inductance decrease with the large gap values. First, we can notice that all the results of the coupling coefficient and mutual inductance appear similar.

The combination that gives the best coupling coefficient, mutual inductance, and coil inductance values is the rectangular shape for the combination of the transmitting and receiving coils. Moreover, for different coil combinations, the circular and the rectangular coils present the best results among all the combinations.

The inductance of the transmitting coil of all cases stays almost constant, but the inductance of the receiving coil experiences a change when the gap value is large.

Table 14. The simulation results of coupling coefficient and mutual inductance for the nine models.

Gap (mm)	k_{cc}	M_{cc}	k_{cr}	M_{cr}	k_{ch}	M_{ch}
50	0.063451	445.95400	0.065329	495.42490	0.060109	419.31340
100	0.008412	59.199180	0.008936	68.025210	0.007896	55.203930
150	0.001441	10.143700	0.001542	11.754990	0.001348	9.431740
200	0.000280	1.969708	0.000301	2.284551	0.000261	1.825223
250	0.000049	0.331442	0.000052	0.383236	0.000046	0.307663
300	0.000004	0.017259	0.000000	0.000000	0.000002	0.001061
Gap (mm)	k_{rc}	M_{rc}	k_{rr}	M_{rr}	k_{rh}	M_{rh}
50	0.065505	495.41300	0.068109	556.24340	0.061977	466.09330
100	0.008969	67.930470	0.009552	78.193680	0.008407	63.302460
150	0.001549	11.742200	0.001664	13.567360	0.001436	10.815340
200	0.000300	2.273186	0.000319	2.609366	0.000274	2.056993
250	0.000052	0.383192	0.000054	0.427079	0.000046	0.336436
300	0.000000	0.000683	0.000000	0.000000	0.000007	0.004216
Gap (mm)	k_{hc}	M_{hc}	k_{hr}	M_{hr}	k_{hh}	M_{hh}
50	0.059890	419.45510	0.061691	466.33140	0.057182	397.82520
100	0.007873	55.215220	0.008418	63.560160	0.007409	51.661350
150	0.001344	9.433949	0.001449	10.999020	0.001265	8.812501
200	0.000261	1.829159	0.000283	2.135191	0.000246	1.712719
250	0.000045	0.306498	0.000050	0.361493	0.000043	0.290551
300	0.000001	0.000207	0.000002	0.001336	0.000003	0.001513

Table 15. The simulation results of transmitting and receiving coil inductance for the nine models.

Gap (mm)	L_{1cc}	L_{2cc}	L_{1cr}	L_{2cr}	L_{1ch}	L_{2ch}
50	6.781647	7.284003	6.784100	8.477065	6.785677	7.171434
100	6.785520	7.298441	6.808041	8.512145	6.801473	7.186742
150	6.785848	7.303122	6.812742	8.525414	6.804330	7.192457
200	6.785000	7.293397	6.801984	8.493260	6.789216	7.182279
250	6.781005	6.781653	6.794038	7.847548	6.786111	6.732637
300	6.773379	2.663993	6.768822	0.000010	6.769274	0.054358
Gap (mm)	L_{1rc}	L_{2rc}	L_{1rr}	L_{2rr}	L_{1rh}	L_{2rh}
50	7.840692	7.295153	7.859934	8.485935	7.861151	7.194426
100	7.844392	7.312895	7.852931	8.533822	7.871329	7.203291
150	7.857680	7.312504	7.833186	8.488914	7.867516	7.205843
200	7.859005	7.295325	7.866308	8.498958	7.859830	7.179874
250	7.853460	6.789841	7.866581	7.867194	7.859914	6.735969
300	7.833505	0.015037	7.844216	0.000008	7.843801	0.052946
Gap (mm)	L_{1hc}	L_{2hc}	L_{1hr}	L_{2hr}	L_{1hh}	L_{2hh}
50	6.720312	7.299205	6.733408	8.486042	6.739215	7.182131
100	6.727379	7.311488	6.714745	8.489664	6.753153	7.200412
150	6.728282	7.317937	6.751840	8.532690	6.738836	7.202593
200	6.730501	7.319607	6.717073	8.472698	6.734780	7.186359
250	6.718816	6.790786	6.761878	7.865598	6.749549	6.735351
300	6.709978	0.015512	6.707614	0.050624	6.705435	0.052990

These results open up potential discussions about the performance of these three shapes according to other variations. Likewise, the rectangular coil shape presents greater horizontal tolerance compared to the circular one and the hexagonal coil shape presents the maximum power transfer efficiency at the central position [36]. Therefore, pad design remains an important field to research.

5. Conclusions

This paper discusses the wireless transfer coil system and the factors that affect ot. The following points were discussed: first, the influence of adding a ferrite core and aluminum sheet to the coil system is discussed. The result shows that the ferrite and aluminum are necessary to guide the magnetic flux, reduce the leakage flux, protect the users around the charging operation, and meet ICNIRP limits. Second, the large air gap reduces the coupling coefficient and mutual inductance values. The main challenge while designing the wireless charger for the electric vehicle is the distance limitation between the transmitting coupler and receiving coupler. This distance depends on the electric vehicle ground clearance and the specifications given by SAE J2954 standard. Third, the coil parameters such as inner radius and number of turns have a significant effect on the system coupling, self-inductance, and mutual inductance. The largest coil inner radius and coil number of turns give the best values of k, L_1, L_2, and M. However, the space taken up by the receiving coil in the vehicle chassis is limited, and the coil cannot be totally increased even if the large inner radius gives good results. Finally, the comparison of three shapes, including ferrite and aluminum, gives priority to the rectangular shape, with a small difference compared to the circular and hexagonal shapes. Thus, several coil possibilities can be encountered during the wireless charging operation. In our case, with the use of the three coil shapes, circular, rectangular, and hexagonal, the combination of circular and rectangular coil gives the best results.

Further research could concentrate on the three-coil structure and the effect of the variation of its main parameters and the shape and the size of the ferrite core and aluminum sheet on the system efficiency for bidirectional WPT system application. Moreover, the human safety issue must be taken into consideration during the design process, especially when the power transfer is increased.

Author Contributions: This paper was developed by a research team from ISA Laboratory; conceptualization, methodology, and formal analysis, T.B. and H.E.F.; software, T.B. and A.L.; investigation and resources, T.B., A.L., O.A., and S.N.; writing, T.B.; review and supervision, H.E.F. All authors have read and agreed to the published version of the manuscript.

Funding: The authors gratefully acknowledge the support of the Moroccan Research Institute for Solar Energy and New Energies (IRESEN) under the grant "INNO-PROJECT 2018/CBSCVEV2X".

Conflicts of Interest: The authors declare no conflict of interest.

References

1. Lassioui, A.; Fadil, H.E.; Belhaj, F.Z.; Rachid, A. Battery Charger for Electric Vehicles Based ICPT and CPT-A State of the Art. In Proceedings of the 2018 Renewable Energies, Power Systems Green Inclusive Economy (REPS-GIE), Casablanca, Morocco, 23–24 April 2018; pp. 1–6.
2. Bouanou, T.; Fadil, H.E.; Lassioui, A. Analysis and Design of Circular Coil Transformer in a Wireless Power Transfer System for Electric Vehicle Charging Application. In Proceedings of the 2020 International Conference on Electrical and Information Technologies (ICEIT), Rabat, Morocco, 4–7 March 2020; IEEE: Rabat, Morocco, 2020; pp. 1–6.
3. Kim, J.; Kim, J.; Kong, S.; Kim, H.; Suh, I.-S.; Suh, N.P.; Cho, D.-H.; Kim, J.; Ahn, S. Coil Design and Shielding Methods for a Magnetic Resonant Wireless Power Transfer System. *Proc. IEEE* **2013**, *101*, 1332–1342. [CrossRef]
4. Kurs, A.; Karalis, A.; Moffatt, R.; Joannopoulos, J.D.; Fisher, P.; Soljačić, M. Wireless Power Transfer via Strongly Coupled Magnetic Resonances. *Science* **2007**, *317*, 83–86. [CrossRef] [PubMed]
5. Budhia, M.; Covic, G.A.; Boys, J.T. Design and Optimization of Circular Magnetic Structures for Lumped Inductive Power Transfer Systems. *IEEE Trans. Power Electron.* **2011**, *26*, 3096–3108. [CrossRef]
6. Budhia, M.; Covic, G.; Boys, J. A New IPT Magnetic Coupler for Electric Vehicle Charging Systems. In Proceedings of the IECON 2010—36th Annual Conference on IEEE Industrial Electronics Society, Glendale, AZ, USA, 7–10 November 2010; pp. 2487–2492.
7. Deng, J.; Li, W.; Nguyen, T.D.; Li, S.; Mi, C.C. Compact and Efficient Bipolar Coupler for Wireless Power Chargers: Design and Analysis. *IEEE Trans. Power Electron.* **2015**, *30*, 6130–6140. [CrossRef]
8. Patil, D.; McDonough, M.K.; Miller, J.M.; Fahimi, B.; Balsara, P.T. Wireless Power Transfer for Vehicular Applications: Overview and Challenges. *IEEE Trans. Transp. Electrification* **2018**, *4*, 3–37. [CrossRef]
9. Bi, Z.; Kan, T.; Mi, C.C.; Zhang, Y.; Zhao, Z.; Keoleian, G.A. A Review of Wireless Power Transfer for Electric Vehicles: Prospects to Enhance Sustainable Mobility. *Appl. Energy* **2016**, *179*, 413–425. [CrossRef]
10. Bosshard, R.; Mühlethaler, J.; Kolar, J.W.; Stevanović, I. Optimized Magnetic Design for Inductive Power Transfer Coils. In Proceedings of the 2013 Twenty-Eighth Annual IEEE Applied Power Electronics Conference and Exposition (APEC), Long Beach, CA, USA, 17–21 March 2013; pp. 1812–1819.
11. Shi, X.; Qi, C.; Qu, M.; Ye, S.; Wang, G.; Sun, L.; Yu, Z. Effects of Coil Shapes on Wireless Power Transfer via Magnetic Resonance Coupling. *J. Electromagn. Waves Appl.* **2014**, *28*, 1316–1324. [CrossRef]
12. Chatterjee, S.; Iyer, A.; Bharatiraja, C.; Vaghasia, I.; Rajesh, V. Design Optimisation for an Efficient Wireless Power Transfer System for Electric Vehicles. *Energy Procedia* **2017**, *117*, 1015–1023. [CrossRef]
13. Yang, Y.; Cui, J.; Cui, X. Design and Analysis of Magnetic Coils for Optimizing the Coupling Coefficient in an Electric Vehicle Wireless Power Transfer System. *Energies* **2020**, *13*, 4143. [CrossRef]
14. Chen, W.; Liu, C.; Lee, C.H.T.; Shan, Z. Cost-Effectiveness Comparison of Coupler Designs of Wireless Power Transfer for Electric Vehicle Dynamic Charging. *Energies* **2016**, *9*, 906. [CrossRef]
15. Ongayo, D.; Hanif, M. Comparison of Circular and Rectangular Coil Transformer Parameters for Wireless Power Transfer Based on Finite Element Analysis. In Proceedings of the 2015 IEEE 13th Brazilian Power Electronics Conference and 1st Southern Power Electronics Conference (COBEP/SPEC), Fortaleza, Brazil, 29 November–2 December 2015; pp. 1–6.
16. Knaisch, K.; Springmann, M.; Gratzfeld, P. Comparison of Coil Topologies for Inductive Power Transfer under the Influence of Ferrite and Aluminum. In Proceedings of the 2016 Eleventh International Conference on Ecological Vehicles and Renewable Energies (EVER), Monte Carlo, Monaco, 6–8 April 2016; pp. 1–9.
17. Knaisch, K.; Gratzfeld, P. Comparison of Magnetic Couplers for Inductive Electric Vehicle Charging Using Accurate Numerical Simulation and Statistical Methods. In Proceedings of the 2015 5th International Electric Drives Production Conference (EDPC), Nuremberg, Germany, 15–16 September 2015; pp. 1–10.
18. Aydin, E.; Kosesoy, Y.; Yildiriz, E.; Aydemir, M.T. Comparison of Hexagonal and Square Coils for Use in Wireless Charging of Electric Vehicle Battery. In Proceedings of the 2018 International Symposium on Electronics and Telecommunications (ISETC), Timisoara, Romania, 8–9 November 2018; pp. 1–4.
19. J2954 (WIP) Wireless Power Transfer for Light-Duty Plug-in/Electric Vehicles and Alignment Methodology-SAE International. Available online: https://www.sae.org/standards/content/j2954/ (accessed on 7 September 2020).
20. Kim, J.; Choi, W.-S.; Jeong, J. Loop Switching Technique for Wireless Power Transfer using Magnetic Resonance Coupling. *Prog. Electromagn. Res.* **2013**, *138*, 197–209. [CrossRef]
21. Beh, T.C.; Kato, M.; Imura, T.; Oh, S.; Hori, Y. Automated Impedance Matching System for Robust Wireless Power Transfer via Magnetic Resonance Coupling. *IEEE Trans. Ind. Electron.* **2013**, *60*, 3689–3698. [CrossRef]

22. Siqi, L.; Mi, C.C. Wireless Power Transfer for Electric Vehicle Applications. *IEEE J. Emerg. Sel. Top. Power Electron.* **2015**, *3*, 4–17. [CrossRef]
23. Lassioui, A.; Fadil, H.E.; Rachid, A.; Belhaj, F.Z.; Tarkany, O.; Bajit, A. Characterestics Analysis of Wireless Power Transfer System for Electric Vehicle Charging Applications. In Proceedings of the 2018 International Symposium on Advanced Electrical and Communication Technologies (ISAECT), Rabat, Morocco, 21–23 November 2018; pp. 1–6.
24. Machura, P.; Li, Q. A Critical Review on Wireless Charging for Electric Vehicles. *Renew. Sustain. Energy Rev.* **2019**, *104*, 209–234. [CrossRef]
25. Lee, S.; Lee, B.; Lee, J. A New Design Methodology for a 300-KW, Low Flux Density, Large Air Gap, Online Wireless Power Transfer System. *IEEE Trans. Ind. Appl.* **2016**, *52*, 4234–4242. [CrossRef]
26. Elnail, K.; Huang, X.; Xiao, C.; Tan, L.; Haozhe, X. Core Structure and Electromagnetic Field Evaluation in WPT Systems for Charging Electric Vehicles. *Energies* **2018**, *11*, 1734. [CrossRef]
27. Ding, W.; Wang, X. Magnetically Coupled Resonant Using Mn-Zn Ferrite for Wireless Power Transfer. In Proceedings of the 2014 15th International Conference on Electronic Packaging Technology, Chengdu, China, 12–15 August 2014; pp. 1561–1564.
28. Bima, M.E.; Bhattacharya, I.; Hasan, S.R. Comparative Analysis of Magnetic Materials, Coil Structures and Shielding Materials for Efficient Wireless Power Transfer. In Proceedings of the 2019 IEEE International Symposium on Electromagnetic Compatibility, Signal Power Integrity (EMC+SIPI), New Orleans, LA, USA, 22–26 July 2019; pp. 95–100.
29. ICNIRP | LF (1 Hz–100 KHz). Available online: https://www.icnirp.org/en/frequencies/low-frequency/index.html (accessed on 6 September 2020).
30. Geselowtiz, D.B.; Hoang, Q.T.N.; Gaumond, R.P. The Effects of Metals on a Transcutaneous Energy Transmission System. *IEEE Trans. Biomed. Eng.* **1992**, *39*, 928–934. [CrossRef]
31. Kim, S.; Park, H.-H.; Kim, J.; Kim, J.; Ahn, S. Design and Analysis of a Resonant Reactive Shield for a Wireless Power Electric Vehicle. *IEEE Trans. Microw. Theory Tech.* **2014**, *62*, 1057–1066. [CrossRef]
32. Dolara, A.; Leva, S.; Longo, M.; Castelli-Dezza, F.; Mauri, M. Coil Design and Magnetic Shielding of a Resonant Wireless Power Transfer System for Electric Vehicle Battery Charging. In Proceedings of the 2017 IEEE 6th International Conference on Renewable Energy Research and Applications (ICRERA), San Diego, CA, USA, 5–8 November 2017; IEEE: San Diego, CA, USA, 2017; pp. 200–205.
33. Xu, D.; Zhang, Q.; Li, X. Implantable Magnetic Resonance Wireless Power Transfer System Based on 3D Flexible Coils. *Sustainability* **2020**, *12*, 4149. [CrossRef]
34. Mohan, S.S.; del Mar Hershenson, M.; Boyd, S.P.; Lee, T.H. Simple Accurate Expressions for Planar Spiral Inductances. *IEEE J. Solid-State Circuits* **1999**, *34*, 1419–1424. [CrossRef]
35. Jow, U.-M.; Ghovanloo, M. Design and Optimization of Printed Spiral Coils for Efficient Transcutaneous Inductive Power Transmission. *IEEE Trans. Biomed. Circuits Syst.* **2007**, *1*, 193–202. [CrossRef] [PubMed]
36. Panchal, C.; Stegen, S.; Lu, J. Review of Static and Dynamic Wireless Electric Vehicle Charging System. *Eng. Sci. Technol. Int. J.* **2018**, *21*, 922–937. [CrossRef]